Characterization of buried cables and pipes using electromagnetic induction loop-loop frequency-domain devices

Julien Thiesson, Alain Tabbagh, Michel Dabas, Antoine Chevalier

Characterization of buried cables and pipes using electromagnetic induction (EMI) loop-loop frequency domain devices

J. Thiesson, A. Tabbagh, M. Dabas, A. Chevalier

ABSTRACT

The detection and characterization of buried cables and metal pipes has become a key component of field surveys carried out prior to excavation work on construction sites. The very high conductivity and magnetic permeability contrast between any buried cables/pipes compared to the soil makes electromagnetic induction (EMI) instruments very useful for their detection. We present a semi-numerical method that can be used to model the responses of this type of target. A straight horizontal conductor is equivalent to a series of magnetic dipoles, the magnitude of which can be determined in the spectral domain and then converted back into the spatial domain through the use of an inverse fast Fourier transform. Simulations and case studies allow to establish rules of thumb for the estimate of (1) the nature of the metal: the in-phase response of magnetic cables is of opposite sign from the conducting ones, (2) the sensitivity to the target characteristic: the influence of the cable/pipe diameter being greater than that of the metal properties, (3) the depth of cables. The simulations also underline the role of the coil configuration: VCP and PERP responses allow a more precise location of the cable/pipe, while the HCP response is less dependent on the orientation. As ground truth, a known electric cable buried at a depth of 0.5m and of 0.002 m diameter was determined at 0.56 m. The first field test is related to the detection of a buried military cable from WWI, between 2.5 m and 3m below the original ground level. The second field test is related to the detection of a water pipe 0.35 m deep. The modelling technique can be applied

to all EM induction prospecting methods and thus opens the way to the correction of the disturbances generated by cables and pipes.

Keywords: electromagnetic methods, near surface, frequency domain EMI, metallic targets, cables, pipes

INTRODUCTION

Among the various types of target studied in near-surface exploration, metallic objects or features are of strong specific interest. The anomalies associated to these features are encountered in a large panel of electromagnetic and magnetic surveys (like land development, UXO detection, archaeological surveying). From the archaeological perspective, metallic objects are man-made items that provide direct insight into the activities practiced by ancient cultures (Tabbagh and Verron 1983), dating back to the Chalcolithic period (beginning approximately 7000 years ago in the Middle East). From the perspective of safety, when new installations or construction sites are envisaged, the terrain must be characterized as accurately as possible and dangerous metallic objects must be carefully removed. Even when frequency-domain electromagnetic (FDEM) methods are used to map out variations in the ground's conductivity, it is not uncommon to observe the presence of unexpected metallic targets. The purpose of this paper is to present a modelling technique for long, conductive and magnetic objects such as metallic cables and pipes. A very simple modelling can be used in the case of a uniform primary magnetic field (Guérin et al., 1994) but for a dipole transmitter the problem is more complex. Our goal is that through a rapid computation, it can be easily applied whenever an accurate determination of the depth and section of long metallic features is required whatever the orientation of the transmitter coil.

MODELLING THE ELECTROMAGNETIC RESPONSE OF A STRAIGHT, HORIZONTAL, CONDUCTIVE AND MAGNETIC STRUCTURE BURIED IN A HOMOGENEOUS GROUND

Here, we consider the basic configuration of so-called EMI electromagnetic devices, whose transmitter (Tx) is a small coil, which can be modeled as a magnetic dipole source, and whose receiver (Rx) is another small loop located at a distance L from the transmitter. Both coils are positioned at a small height d above the surface of the ground (Figure 1), and the apparatus is moved in the (x, y) plane, x being the direction parallel to the Tx and Rx line. For simplicity, and because of the very large contrast in electromagnetic properties between the cable and its surroundings, we assume the ground to be homogeneous. The technique, however, can easily be extended to a 1D layered ground. As the transmitter is a point source, the primary EM field diffusing through the ground varies strongly along the length of a horizontally aligned cable or pipe positioned at a depth z_c. The ratio between the cable length and L is sufficiently large for the length to be considered as infinite. The cable orientation, x' (unknown by the prospector), differs by an angle α from x, consequently while the device position is defined in the (x, y, z) coordinate system the cable description takes place in the (x', y', z) coordinate system (Figure 1).

For UXO modeling there exists in the literature a significant number of papers considering the responses of a body of revolution of limited length (Wait and Hill, 1973; Shubitidze et al., 2002; Shubitidze et al., 2005); here, due to the extent of the cable it is preferable to adopt the model of a 2D body channeling the induced current (Parry and Ward, 1971; Howard, 1972; Tsubota and Wait, 1980). Our approach continues that of Tabbagh (1977).

In our approach, as a consequence of the electrical conductivity (and when necessary the magnetic permeability) contrast between the surrounding earth and the metal, as well as

75 the small diameter of the cylinder, only one electromagnetic mode can be assumed to induce a
76 significant EM response: this is the $(E_{x'}, H_{y'}, H_z)$ mode, $E_{x'}$ being parallel to the cable. The
77 cable can thus be considered that of a sequence of magnetic dipoles of variable intensity with
78 axes perpendicular to it. We apply a three-step modelling approach: firstly, the primary field
79 components are computed at the cable's location, secondly the dipole strengths induced by the
80 primary field are determined, and finally the secondary field generated by each of the line's
81 dipoles is computed at the receiver location.
82
83 **Field generated in the ground by the dipole transmitter**
84 The analytical expressions for the EM components generated in a layered ground by a
85 vertical or horizontal magnetic dipole positioned in the air above the ground, is well known in
86 the geophysical literature (Tabbagh 1985, Ward and Hohmann 1987). In the following we use
87 the magnetic dipole expressions for a homogeneous ground of electrical conductivity σ and
88 magnetic permeability μ.
89 If the transmitter is a vertical magnetic dipole, M_z, located at a (0, 0, –d) (the z axis
90 points downwards, Figure 1), the magnetic components at the point (x, y, z) are:

91 $$H_x = \frac{M_z}{4\pi}\frac{x}{r}\int_0^\infty \lambda^2 \frac{2\frac{u}{\mu}}{\frac{u}{\mu}+\frac{\lambda}{\mu_0}} e^{-uz}e^{-\lambda d} J_1(\lambda r)d\lambda, \qquad (1)$$

92 $$H_y = \frac{M_z}{4\pi}\frac{y}{r}\int_0^\infty \lambda^2 \frac{2\frac{u}{\mu}}{\frac{u}{\mu}+\frac{\lambda}{\mu_0}} e^{-uz}e^{-\lambda d} J_1(\lambda r)d\lambda \qquad (2)$$

93 $$H_z = \frac{M_z}{4\pi}\int_0^\infty \lambda^2 \frac{2\frac{\lambda}{\mu}}{\frac{u}{\mu}+\frac{\lambda}{\mu_0}} e^{-uz}e^{-\lambda d} J_0(\lambda r)d\lambda \qquad (3)$$

Where J_0 and J_1 are the Bessel functions of the first kind, $r = \sqrt{x^2 + y^2}$, $u = \sqrt{\lambda^2 + \gamma^2}$, (with i^2=-1 and $\gamma^2 = i\sigma\mu\omega$).

If the transmitter is a horizontal magnetic dipole, *Mx*, located at (0, 0, –*d*):

$$H_x = \frac{M_x}{4\pi}\left[\frac{x^2 - y^2}{r^3}\int_0^\infty \lambda \frac{2\frac{u}{\mu}}{\frac{u}{\mu} + \frac{\lambda}{\mu_0}} e^{-uz} e^{-\lambda d} J_1(\lambda r) d\lambda - \frac{x^2}{r^2}\int_0^\infty \lambda^2 \frac{2\frac{u}{\mu}}{\frac{u}{\mu} + \frac{\lambda}{\mu_0}} e^{-uz} e^{-\lambda d} J_0(\lambda r) d\lambda\right] \quad (4)$$

$$H_y = \frac{M_x}{4\pi}\left[\frac{2xy}{r^3}\int_0^\infty \lambda \frac{2\frac{u}{\mu}}{\frac{u}{\mu} + \frac{\lambda}{\mu_0}} e^{-uz} e^{-\lambda d} J_1(\lambda r) d\lambda - \frac{xy}{r^2}\int_0^\infty \lambda^2 \frac{2\frac{u}{\mu}}{\frac{u}{\mu} + \frac{\lambda}{\mu_0}} e^{-uz} e^{-\lambda d} J_0(\lambda r) d\lambda\right] \quad (5)$$

$$H_z = \frac{M_x}{4\pi}\frac{x}{r}\int_0^\infty \lambda^2 \frac{2\frac{\lambda}{\mu}}{\frac{u}{\mu} + \frac{\lambda}{\mu_0}} e^{-uz} e^{-\lambda d} J_1(\lambda r) d\lambda \quad (6)$$

Response of a straight horizontal cable in a varying perpendicular magnetic field

We consider an infinitely long, circular, conductive and magnetic cylinder of radius *a*, conductivity σ_1 and permeability μ_1, such that $\gamma_1^2 = i\sigma_1\mu_1\omega$. As the cylinder is aligned in the *x'* direction we use the *(r, θ, x')* coordinate system, where $r = \sqrt{y'^2 + z^2}$ and θ=0 in the *y'* direction. The external field excitation $H_p(x')$ can be broken down into two components $H_{py'}(x')$ and $H_{pz}(x')$. Due to the small value of *a*, both of these can be considered to be uniform over the section of the cylinder. Due to the linearity of the Maxwell's equation the secondary fields induced by each primary component add. The behavior of the resulting (*Ex'*, *Hy*', *Hz*) EM mode can be calculated using $E_{x'}$, which is defined and continuous everywhere, and verifies the Helmholtz's equation:

$$\frac{1}{r}\frac{\partial}{\partial r}\left(r\frac{\partial E_{x'}}{\partial r}\right) + \frac{1}{r^2}\frac{\partial^2 E_{x'}}{\partial \theta^2} + \frac{\partial^2 E_{x'}}{\partial x'^2} - \gamma^2 E_{x'} = 0 \quad (7)$$

The Fourier transform in the *x'* direction can be written:

$$\hat{E}(r,\theta,\lambda) = \int_{-\infty}^{\infty} E_{x'}(r,\theta,x')e^{-2\pi i\lambda x'}dx' \qquad (8)$$

and expression (7) is thus transformed to:

$$\frac{1}{r}\frac{\partial}{\partial r}\left(r\frac{\partial \hat{E}}{\partial r}\right)+\frac{1}{r^2}\frac{\partial^2 \hat{E}}{\partial \theta^2}-(\gamma^2+4\pi^2\lambda^2)\hat{E}=0 \qquad (9).$$

By defining the variables $\eta_1 = \sqrt{\gamma_1^2 + 4\pi^2\lambda^2}$ inside the cylinder, and $\eta = \sqrt{\gamma^2 + 4\pi^2\lambda^2}$ outside the cylinder, the solutions to equation (9) outside the cylinder are:

$$\hat{E}(r,\theta,\lambda) = \alpha(\lambda)K_1(\eta r)\sin\theta \qquad (10)$$

$$\hat{H}_r(r,\theta,\lambda) = -\frac{1}{i\omega\mu}\alpha(\lambda)K_1(\eta r)\frac{\cos\theta}{r} \qquad (11),$$

$$\hat{H}_\theta(r,\theta,\lambda) = \frac{1}{i\omega\mu}\alpha(\lambda)K_1^{'}(\eta r)\eta\sin\theta \qquad (12)$$

where:

$$\alpha(\lambda) = i\omega\mu\hat{H}_p(\lambda)a\frac{\mu_1-\mu\dfrac{\eta_1 a I_1^{'}(\eta_1 a)}{I_1(\eta_1 a)}}{\mu_1\eta a K_1^{'}(\eta a)-\mu K_1(\eta a)\dfrac{\eta_1 a I_1^{'}(\eta_1 a)}{I_1(\eta_1 a)}} \qquad (13)$$

In the above expressions, $\hat{H}_p(\lambda)$ is the Fourier transform of the primary magnetic field component under consideration, K_1 and I_1 are first order Bessel functions of the second kind, and K_1' and I_1' are their first derivatives, respectively. By identifying the magnetic field expression with those generated by a continuous line of magnetic EM dipoles in a homogeneous ground of σ conductivity and μ magnetic permeability, the linear density of the equivalent magnetic dipole can be written as:

$$\hat{M}(\lambda) = -\frac{2\pi}{i\omega\mu}\frac{\alpha(\lambda)}{\eta} \qquad (15).$$

An inverse Fourier transform can then be used to calculate *M(x')*.

Secondary magnetic field generated by a line of dipoles

The total field strength at the receiver is computed by summing the fields generated by each of the dipoles, using the same analytical expressions as those presented in equations (1) to (6). Practically the total length of the cable is chosen greater than ten times the inter-coil separation, and this length is regularly (because of the use of a FFT software) divided into small elements the length of which being small against both the depth of the cable and the inter-coil separation: for instance, if L=1.18 m and z_c=0.5 m one can choose a 15 m length divided into $\delta x'$=0.05 m elements.

The target response adds to that of the soil and can be expressed either in terms of H_s/H_p ratio (where H_s is the total secondary field generated by the underground in response to the primary field, H_p, generated by the transmitter) or in terms of apparent soil magnetic susceptibility and electrical conductivity (the susceptibility and conductivity respectively of a homogeneous ground giving the same total response in-phase and quadrature response respectively) variation (Thiesson et al., 2014). The apparent magnetic susceptibility and apparent conductivity are significant because the relative variation of each apparent property allows a direct assessment of the detectability of a target.

SYNTHETIC RESPONSES OBTAINED WITH DIFFERENT INSTRUMENT CONFIGURATIONS

Nonmagnetic cable

We consider a non-magnetic, conductive cable having an equivalent radius of 0.002 m and a conductivity of 0.596 x 10^8 Sm^{-1}, buried at a depth of 0.5 m in ground characterized by a resistivity of 100 Ωm and a magnetic susceptibility equal to 50 10^{-5} SI. The cable's response is computed and plotted for the three most common configurations: vertical coplanar (VCP),

horizontal coplanar (HCP), and perpendicular (PERP), for the case of a device operated at 9 kHz, with L=2 m and d=0.2 m. For each configuration, the response measured by the device is the complex ratio of the secondary field measured by the receiver, to the static primary field at the receiver's location, $H_p = \frac{1}{4\pi}\frac{M}{L^3}$. These responses depend on the relative orientation of the instrument (x direction defined by the line joining the transmitter, Tx, to the receiver, Rx) with respect to that of the cable, x' direction. The measurement is plotted at the mid-point between Tx and Rx. In Figure 2 we show the in-phase and quadrature responses (in ppt) for y' directed profiles perpendicular to the cable, when the Tx - Rx line is aligned at an angle of 0° (broadside array), 30°, 60° and 90° (in line profile) with respect to the cable.

Figure 2 clearly shows that, for all configurations, the in-phase response is significantly greater (more than twice as strong) than the quadrature response. The cable's presence produces a decrease in the apparent magnetic susceptibility of the ground (numerical values are provided in Table 1). A very strong dependence on angular alignment can also be observed: the VCP response is greatest when the angle is small and weakest at larger angles. The central response changes in sign when the instrument/cable alignment reaches an angle of approximately 45°. In the case of the HCP response, the orientation of the instrument with respect to the cable influences mainly the width of the central anomaly, with its amplitude and sign remaining similar in value. The PERP response is inherently asymmetric with complex changes in sign; it exhibits significant amplitudes for all instrument-cable orientations. The greatest amplitude occurs when the instrument is parallel to the cable (broadside array) and the response is then symmetric. Contrary to the VCP and HCP responses, there can be a significant lateral offset between the maximum response and the cable's horizontal position: the response maximum is shifted towards the horizontal dipole (the receiver in the case of a vertical transmitter, the transmitter in the case of a vertical receiver), by a distance of approximately 0.5 m for the parameter values used in the present example.

There is a significant decrease in response with cable depth, as shown by the data provided in Table 1 for a 10° cable orientation, and in Table 2 for an 80° cable orientation. If one fixes the detection limit to 10% of the total response (sum of the responses generated by soil conductivity and susceptibility and of the cable response), none of the configurations allow the cable to be detected at a depth greater than 2 m. At 1 m, this is also found to be impossible to detect in the case of the HCP response which, as for other types of 3D feature (Tabbagh 1986), is characterized by a change in sign at a certain depth (depending on L, between 0.5 and 2 m in the present case): a triple peak response, with a pronounced maximum (in Hs/Hp), is observed at the center of the profile, in the case of a small cable depth, whereas a single central minimum is observed at greater cable depths. In the case of the VCP response, detection of the cable at a depth of 1 m is possible only when the instrument is aligned nearly parallel to the cable (broadside array). In the case of the PERP response, detection is possible at a depth of 1 m, for all instrument orientations: this outcome is in agreement with the results of a previous study (Tabbagh 1986) dealing with the detection of metallic objects and 3D features. It is important to note that, when compared to smaller values of L, when the cable is at a depth of 2 m, the conductivity response of the ground itself is significantly amplified such that any change in the cable's equivalent apparent conductivity (quadrature responses) remains very small, and undetectable. This is not the case for the in-phase responses, in which the magnetic susceptibility response of the surrounding soil does not increase with L. To facilitate the comparison between the three coil configurations, the decreased responses versus depth of maximum of the absolute value of the in-phase responses are drawn in Figure 3, the responses being expressed in proportion of the ground in-phase responses for a broadside array position of the instrument.

A few basic guidelines can be established from these simulated case studies, for the assessment of a cable's depth: these are based on the presence or absence of alternating peaks

in the responses and, when two (or more) different values of L can be used, on the ratio between the peak levels observed at these different distances. As the distance between the peaks depends not only on the inter-coil separation, but also on the orientation of the instrument with respect to the cable, it cannot be easily used to determine the depth of the cable. However, in the case of the VCP response, for which the anomaly is most often a single peak, a triple peak occurs in the presence of very superficial cables when $z_c + d \leq 0.18L$. In the case of the HCP response, the change in shape of the anomaly, from a triple to a single peak, takes place when $z_c + d \cong 0.7L$. In the case of the PERP response, when the orientation of the instrument is nearly perpendicular to that of the cable, the transition between a triple peak anomaly (superficial cable) and a single peak anomaly (deeper cable) occurs when $z_c + d \cong 0.5L$.

The dependences of the response on the diameter of the cable and on the metal conductivity are not linear and significantly different. This difference is illustrated in Figure 4 where are drawn the variations of the maximum of the response for a VCP configuration (in broadside array position to get the simplest anomaly shape). In figure 4a one observes that for lower diameters the diameter influence is limited but above 7 mm its role becomes very strong. On the contrary in Figure 4b the variation of the response with the metal conductivity remains small. This can be explained by the fact that whatever the metal conductivity (or the magnetic permeability see below) the property contrast with the surrounding soil stays very huge.

Magnetic cable

Although conductive wires are usually made from non-magnetic copper and buried pipes in lead, buried cables are often protected by external steel sheaths, which generate a response to an applied electromagnetic field. In order to assess the role of such a magnetic

cable sheath, we thus consider the same ground, instruments, cable orientations and depth as in the example provided in Figure 2, associated with a lower electrical conductivity, i.e. 0.6 x 10^7 Sm^{-1}, and a relative magnetic permeability given by μ_r=100. As shown in Figure 5, due to the huge property contrast, the absolute values of the magnitude of the responses do not differ from more than 30% from those of Figure 2. However, when compared to the case of a non-magnetic cable, the in-phase responses are of the opposite sign, whereas the sign of the quadrature responses does not change. This behavior can be used as a relevant criterion, to distinguish between these two different types of target. As in the case of the non-magnetic cable, the VCP response is highly sensitive to the instrument's orientation with respect to the cable, and the HCP response exhibits changes in the width of the anomaly. There is also a strong decrease in response depth: with the PERP configuration, for a cable depth of 1 m, the maximum response is 0.040 ppt, whereas it reaches just 0.0068 ppt at a depth of 2 m.

For the purpose of comparison, in a magnetic survey where the total field gradient is measured between two sensors located at heights of 0.3 and 0.8 m above the ground, the same cable located at a depth of 0.5 m would have produced a maximum anomaly of 17 nTm^{-1} (without considering any possible remanent magnetization effect). For a cable at a depth of 2 m, although the anomaly would be reduced to 1.8 nTm^{-1}, it would still remain detectable.

The responses here obtained for straight horizontal very small diameter cylindrical bodies are in fine accordance with the extensive results published for various types of simple target such as conductive dipping plates, spheres or prismatic bodies (Frischknecht et al. 1991).

FIELD EXAMPLES

Characterization of an already known cable

This electric power cable has been installed in a garden at 0.5 m depth. The average resistivity value of the soil is 100Ω.m. The cable is comprised of 5 copper wires of 2.5 mm^2 section; the total section is thus 12.5 mm^2 and an equivalent radius of 2 mm can be expected. The CMD (Gf Instruments, Brno) instrument was used in VCP configuration. This instrument operates at one frequency, 30 kHz, and has one transmitting coil and three receiving coils at distances of L=0.32, 0.71 and 1.18 m from the transmitting coil. All of the coils are coplanar, and measurements can be made in either the horizontal coplanar (HCP), or the vertical coplanar (VCP) configurations. The sensitivity displayed by the instrument data record is 0.01 ppt but additional field and acquisition noises will make that number higher. The cable anomaly cannot be observed for L=0.32 m, but it is clearly marked for both 0.71 m and 1.18 m separations. Figure 6 illustrates the comparison between the raw data and the inversion results for a copper cable of 0.002 m radius located at 0.56 m depth in good agreement with the expected characteristics of the cable.

Military cable dating from World War I

A survey was carried out in Artois (France), in order to locate underground relics dating from the First World War, at a site designated for a new housing development. These relics can correspond to several types of metallic object (including UXO), as well as underlying tunnels or bunkers. In this area, the superficial formation is silty (mainly loess), and its electrical resistivity varies between 50 and 60 Ωm. After removing the first two soil horizons a DualEM 421S EMI device was used in the continuous profiling mode, with a 1m separation between profiles, and a 0.3m sampling interval along the profiles. The exact location of each measurement was recorded by means of a differential GPS. The instrument was towed behind a small vehicle, with a clearance of 0.315 m above the flat ground surface.

The DualEM 421S is a single frequency (9 kHz), multi-receiver EMI instrument (DualEM Ltd, Milton, Ontario), which associates one horizontal transmitter loop with three pairs of receiver coils. In each coil pair, the first coil is horizontal and in the same plane as the transmitter coil, allowing HCP measurements to be made. For the purposes of PERP measurements, the axis of the second receiver coil is in the same plane as the transmitter coil and aligned radially with respect to the transmitter coil axis. The first pair of receivers is located at respectively 1.0 and 1.1 m from the transmitter, the second pair at 2.0 and 2.1 m, and the third pair at 4.0 and 4.1 m. Thus 12 different responses are measured: 6 in-phase and 6 in quadrature, they provide information concerning ground magnetic susceptibility and electrical conductivity.

A long straight feature was detected crossing the survey area (Figure 7). It was easily interpreted to be a buried cable. To refine the interpretation two smaller zones were selected: 40 x 40 m Zone 1 (Figure 8a), and 28 x 35 m Zone 2 (Figure 8b). As the magnetic map of the whole area (not shown here) does not reveal any corresponding anomaly, it can be assumed that the cable is non-magnetic (i.e. made from copper or aluminum), and that the observed EM responses are indicative of its conductivity.

The measurements were acquired by a series of parallel survey lines that were traversed in alternating directions. In the case of the PERP configuration, as shown in Figure 7, it was thus necessary to split the results into two different maps, one corresponding to the first direction displacements and the other corresponding to alternate direction displacements of the instrument.

As the signals obtained using both the HCP configuration at L=1 m, and the PERP configuration at L=1.1 m are weak and are affected by significant interference from other objects, our interpretations are based on the in-phase data derived from the responses with HCP at 2 m, HCP at 4 m, PERP at 2.1 m and PERP at 4.1 m. The general patterns produced

by the anomaly are very clear in both Zones 1 and 2, as shown in Figures 8a and 8b, which allow the cable's horizontal position and alignment to be identified directly: its azimuth is 85° (east of north) orientated. In the case of these measurements, the instrument orientated at 53° azimuth is aligned at 32° with respect to the cable. Only two further parameters remain to be determined: the depth and, having fixed its conductivity to the one of the copper, the equivalent diameter of the cable. One can expect that the first depends on the lateral extent of the anomaly, while the second of its amplitude.

In Zone 1, considering 20 profiles crossing the cable, we calculated the average profiles for each configuration and searched for the best model fitting with them. The experimental and model curves are presented in Figure 9 where the PERP data exhibit an important noise. The calculated depth of the cable is 1.5 m and the equivalent diameter 10 mm. These results are in fine agreement with the observation of the site developer: between 2.5 and 3 m below the original ground level, that corresponds to 1.5 and 2 m below the measurement surface, and a diameter lesser than 15 mm. In Zone 2, the data and their interpretation lead to very similar results.

Water pipe

During the course of a survey used to map the ancient buildings of a destroyed medieval abbey, a long feature was observed in the in-phase responses detected in the three channels of a CMD (Gf Instruments, Ltd, Brno) slingram EMI device. Figure 10 shows three samples of the survey results produced from the in-phase channels in the VCP configuration. The surveyed area has a 12 Ω.m average apparent resistivity and 40 10^{-5} SI apparent magnetic susceptibility.

Contrary to the preceding case, the location of the instrument was not measured with a dGPS but interpolated along each profile (55 m long) under the hypothesis that the operator

moved along the profile at a constant speed. The maps clearly define the pipe orientation: the instrument is aligned at an angle of 78° relative to the feature. The sign of the anomaly reveals that the pipe is made from a non-magnetic metal, and since it was probably installed during the mid- XX^{th} century, it is likely that lead was used ($\sigma=0.48\ 10^7\ Sm^{-1}$). As the anomaly is very thin for L=0.32 m the interpretation is based on the two greater coil separations only. For the determination of the pipe diameter and depth it is preferable to separately interpret each profile rather than to consider an averaged profile for which the location errors would significantly enlarge the anomaly. This approach allows assessing the variability of the results and thus the robustness and accuracy of the inversion better than by adding any artificial noise. Due to the high sensitivity of the responses to the pipe diameter it must be fixed at 8 mm. With fifteen different profiles the average value of the depth is 0.36 m and the standard deviation 0.056 m. The results obtained at profile 25 are presented in Figure 11.

CONCLUSION

For a long time geophysicists have been aware that the presence of metallic cables or pipes produces EM anomalies. These anomalies can be of great interest for the identification of past human activities as well as being a significant noise source in all EM surveys. The modelling technique described in this paper makes it possible to determine basic characteristics of a buried, linear metallic object such as a cable or a pipe, including its depth and the magnetic/ non-magnetic differentiation.

The complexity of the responses with the relative orientation between the cable/pipe and the instrument is significant and the unavoidable presence of noise in field data amplifies this complexity. Thus it is essential to map the EMI instruments responses. However, it can be wise, after the mapping step, to achieve a single profile perpendicular to the cable/pipe orientation with the instrument parallel to the cable/pipe (broadside array): for such setting the

amplitude is maximal and the unique peak is centered above the target. VCP and PERP configurations would allow a more precise location of the cable/pipe than HCP. For small diameter, with the use of complementary information about the metal type, one can also estimate the diameter. Greater diameters play the major role in the magnitude of the responses whatever the metal conductivity. The buried depth governs the lateral anomaly extent.

Moreover, the proposed modelling technique paves the way to the development of methods allowing the response to cable or pipe, measured using any EM survey method, to be identified and rejected.

ACKNOWLEDGEMENTS

We gratefully acknowledge the kind cooperation and assistance provided by the owners of the land surveyed during our field work and Geocarta-Paris for access to the data. We warmly thank the reviewers, two anonymous and David Fitterman, and the associate editor Erika Gasperikova for their suggestions and language corrections.

REFERENCES

Frischknecht, F. C., V. F. Labson, B. R. Spies, and W. L. Anderson, 1991, Profiling methods using small sources: in Nabighian, M. N., ed. Electromagnetic Methods in Applied Geophysics, Volume 2, Application, Part A, Tulsa, SEG, pp 105-270.

Guérin R., A. Tabbagh, and P. Andrieux, 1994, Field and/or resistivity mapping in MT-VLF and implications for data processing: Geophysics, **59**, 1695-1712.

Howard, A. Q., 1972, The electromagnetic fields of a subterranean cylindrical inhomogeneity excited by a line source: Geophysics, **37,** 975-984.

Parry, J. R., and S. H., Ward, 1971, Electromagnetic scattering from cylinders of arbitrary cross-section in a conductive half-space: Geophysics, **36**, 67-100.

Shubitidze, F., K. O'Neill, S. A. Haider, K. Sun, and K. D. Paulsen, 2002, Application of the method of auxiliary sources to the wide-band electromagnetic induction problem: IEEE transactions on Geoscience and Remote Sensing, **40**, 928-942.

Shubitidze, F., K. O'Neill, I. Shamatava, K. Sun, and K. D. Paulsen, 2005, Fast and accurate calculation of physically complete EMI response by a heterogeneous metallic object: IEEE transactions on Geoscience and Remote Sensing, **43**, 1736-1750.

Tabbagh, A., 1977, Deux nouvelles méthodes géophysiques de prospection archéologique : Thèse, Université Pierre et Marie Curie, Paris.

Tabbagh, A., 1985, The response of a three dimensional magnetic and conductive body in shallow depth E.M. prospecting: Geophysical Journal of the Royal Astronomical Society, **81**, 215-230.

Tabbagh, A., 1986, What is the best coil orientation in the slingram electromagnetic prospecting method? Archaeometry, **28**, 185-196.

Tabbagh, A., and G. Verron, 1983, Etude par prospection électromagnétique de trois sites à dépôts de l'Age du Bronze : Bulletin de la Société Préhistorique Française, **80**, 375-389.

Thiesson, J., P. Kessouri, C. Schamper, and A. Tabbagh, 2014, Calibration of frequency-domain electromagnetic devices used in near-surface surveying: Near Surface Geophysics, **12**, 481-491.

Tsubota, K., and J. R. Wait, 1980, The frequency and time domain response of a buried axial conductor: Geophysics**, 45**, 941-951.

Wait, J. R., and D. A. Hill, 1973, Excitation of a homogeneous conductive cylinder of finite length by a prescribed axial current distribution: Radio Science, **8**, 1169-1176.

Ward S. A., and G. H. Hohmann, 1987, Electromagnetic theory for geophysical applications: in Electromagnetic methods in applied geophysics, volume1, Theory, edited by M. N. Nabighian, SEG, Tusla OK, 131-311.

Figure captions

Figure 1: Coordinate system and cable position: top view and lateral view, Tx transmitting coil, Rx receiving coil, α angle between the instrument orientation and the cable/pipe, d clearance of the instrument above the ground surface and z_c depth of the cable/pipe.

Figure 2: Hs/Hp responses in ppt for profiles perpendicular to a non-magnetic cable (0.002 m radius and 0.596 10^8 Sm^{-1} conductivity, located at a depth of 0.5 m): continuous line for the profile when the angle between the cable and the instrument is equal to 90° (in-line profile), large dashed line for 60°, medium dashed line for 30°, and thin dashed line for 0° (broadside array).

Figure 3: Decrease of maximum of the absolute value of the in-phase response for PERP (solid line), HCP (small-dash line), and VCP (dashed line) versus normalized depth (z_c/L). The responses are expressed in proportion of the respective ground (50 10^{-5} SI magnetic susceptibility) in-phase response for a broadside array position of the instrument (*f*=9 kHz, *d*=0.2 m).

Figure 4: Ratio of H_s/H_p (in ppt) for VCP response when α=0° for *f*=9 kHz, *L*=2 m, *d*=0.2 m, *h*=0.5 m, σ_1=0.596 108 S/m as a function of (a) cable diameter (), (b) metal conductivity for diameter of 0.004 m.

Figure 5: Hs/Hp responses in ppt for profiles perpendicular to a magnetic cable (0.002 m radius, 0.6 10^7 Sm^{-1} conductivity, and 100 relative magnetic permeability, at a depth of 0.5 m): continuous line for the profile when the angle between the cable and the instrument is equal to 90° (inline profile), large dashed line for 60°, medium dashed line for 30° and thin dashed line for 0° (broadside array).

Figure 6: Response (in-phase ratio *Hs/Hp* in ppt) over a known electric power cable: comparison for (a) *L*=0.71 m and (b) *L*=1.18 m between the raw data (solid lines) and the inversion results for a copper cable of 2 mm radius located at 0.56 m depth (dashed lines).

Figure 7: Military cable dating back to World War I. In-phase *Hs/Hp* ratio in ppt. The raw data was acquired along paths whose direction varies by 180° between adjacent profiles. By separating the profiles made with the instrument along southwesterly and northeasterly directions (profile directions are indicated by black arrows), readable maps can be obtained. In the PERP configuration, the response maxima are shifted towards the horizontal sensor for data collected with the DualEM instrument.

Figure 8: Detection of a military cable dating from World War I. Map of the in-phase response for Zones 1 and 2, using the HCP and PERP configurations (a) at L=2 m and 2.1 m respectively, and (b) at L=4 m and 4.1 m respectively, with the DualEM instrument. Profile directions alternate between 85° and 265° (east of north).

Figure 9: Detection of a military cable dating from World War I: comparisons between experimental responses (solid lines) and modeled responses (dashed lines) for (a) HCP L=2 m, (b) HCP L=4 m, (c) PERP L=2.1 m, and (d) L=4.1 m.

Figure 10: Detection of a water pipe: maps of the in-phase responses for the three inter-coil separations of the CMD instrument with VCP configuration for (a) L= 0.32, (b) L=0.71, and (c) L=1.18 m. Profile directions alternate between 150° and 330° (east of north).

Figure 11: Comparisons between experimental responses (solid lines) and modeled responses (dashed lines) at profile 25 for (a) L=0.71 m and (b) L=1.18 m.

Table captions

Table 1: Variations in maximum response and corresponding magnetic susceptibility, as a function of cable depth, for a 10° alignment between the cable and the instrument.

Table 2: Variations in maximum response and corresponding magnetic susceptibility, as a function of cable depth, for an 80° alignment between the cable and the instrument.

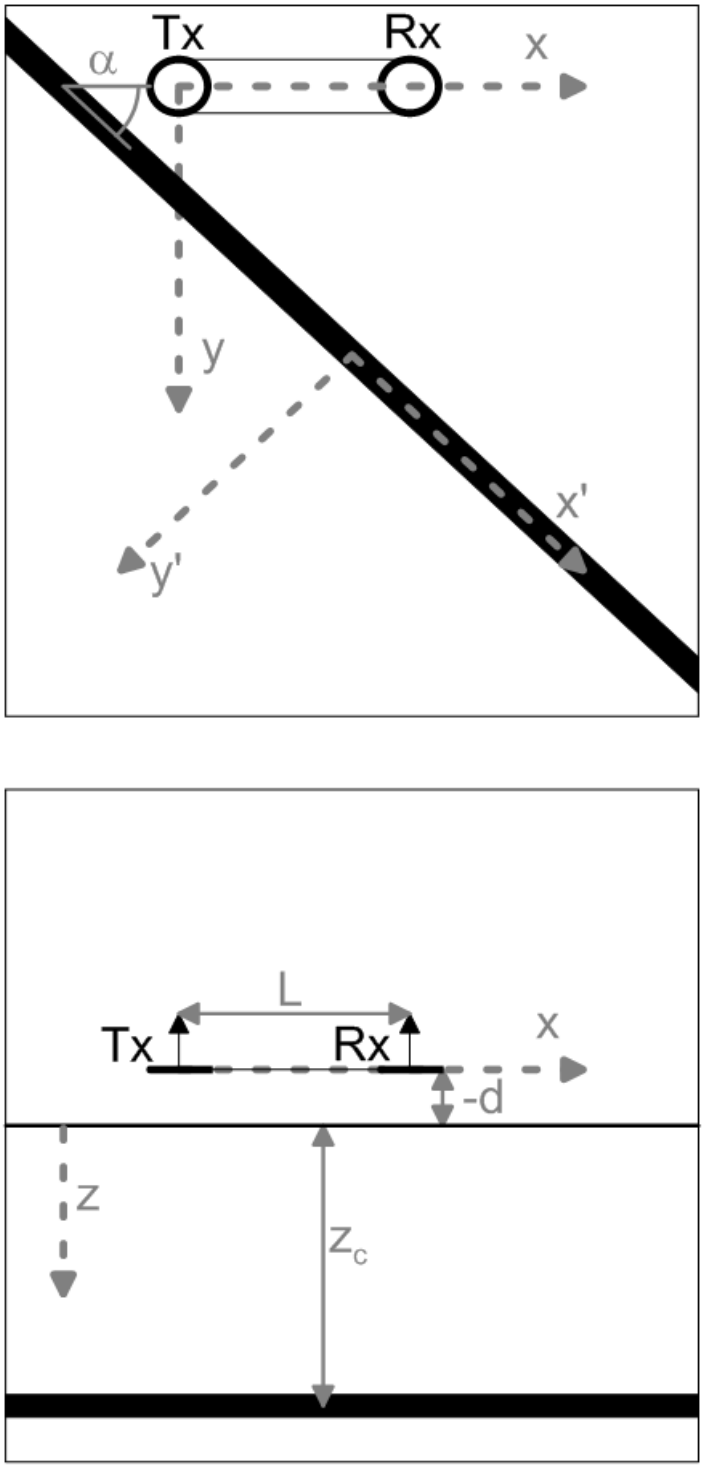

Fig. 1

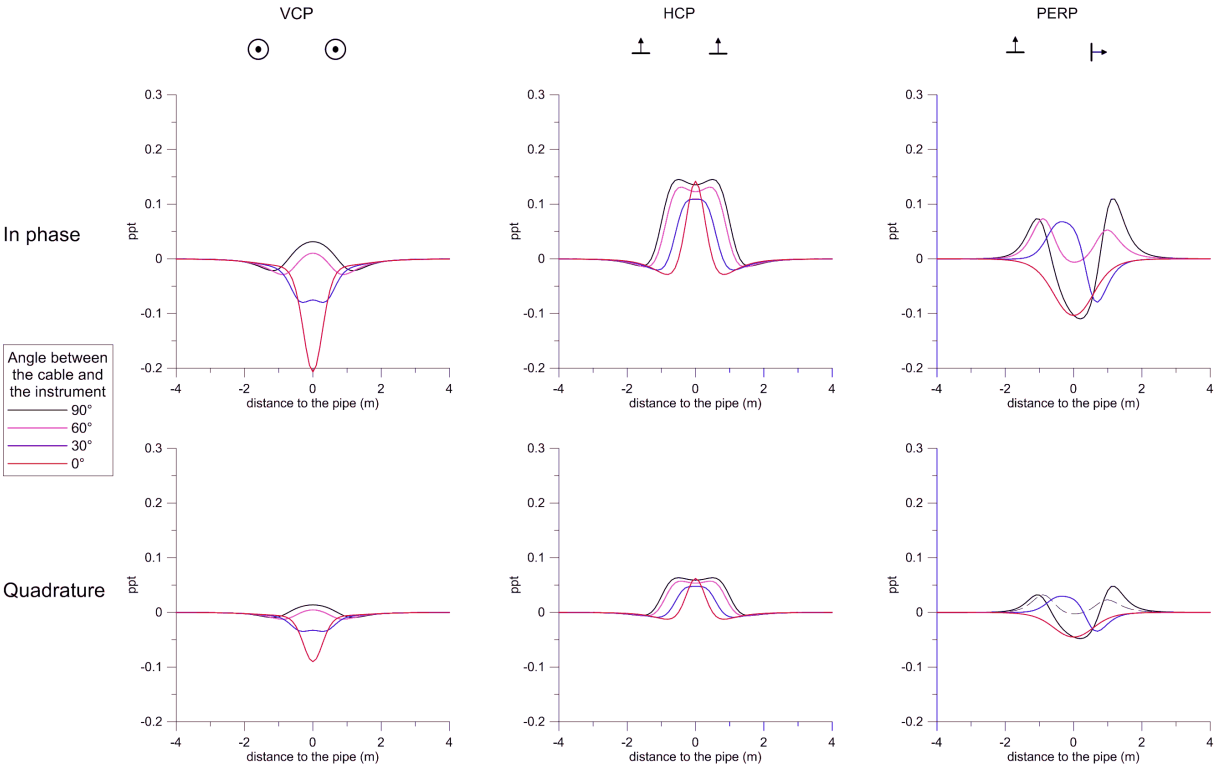

458

459 Fig. 2

460

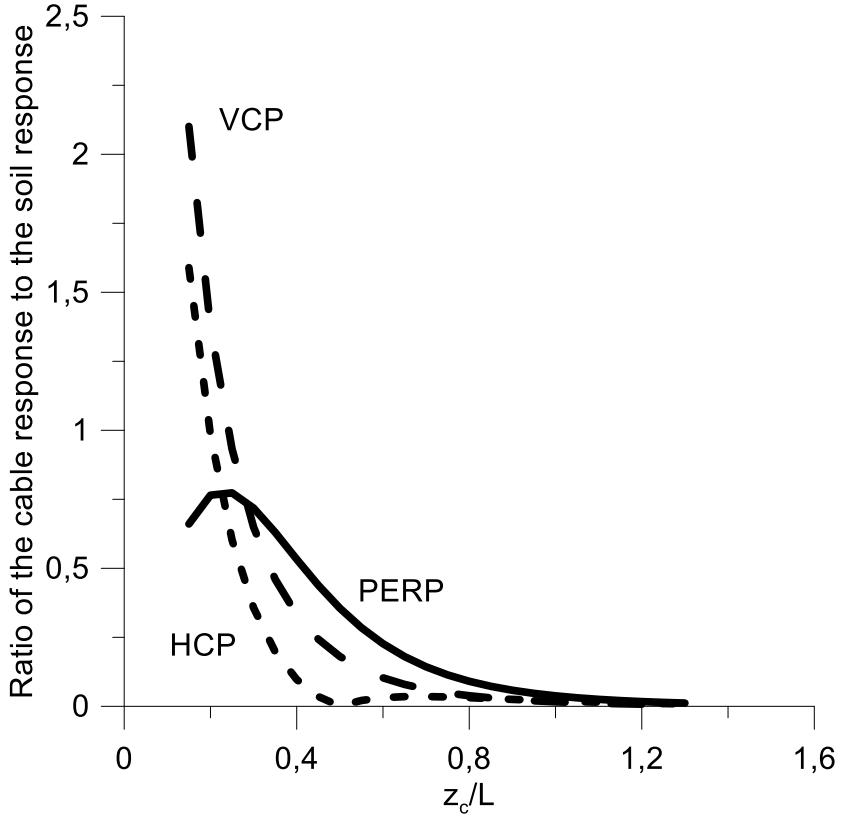

461

462 Fig. 3

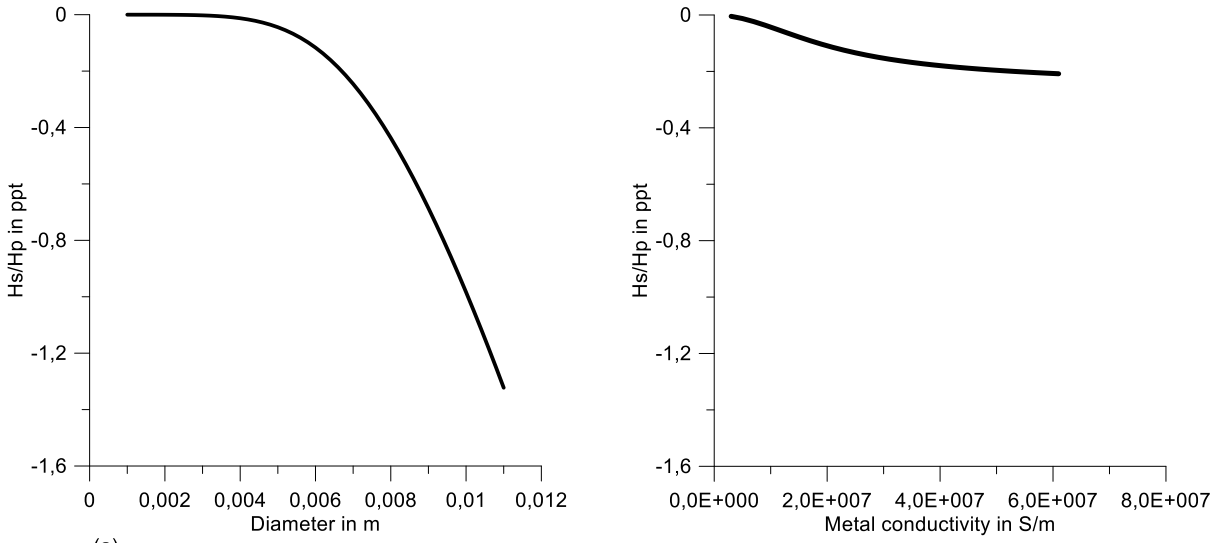

463

464 Fig. 4

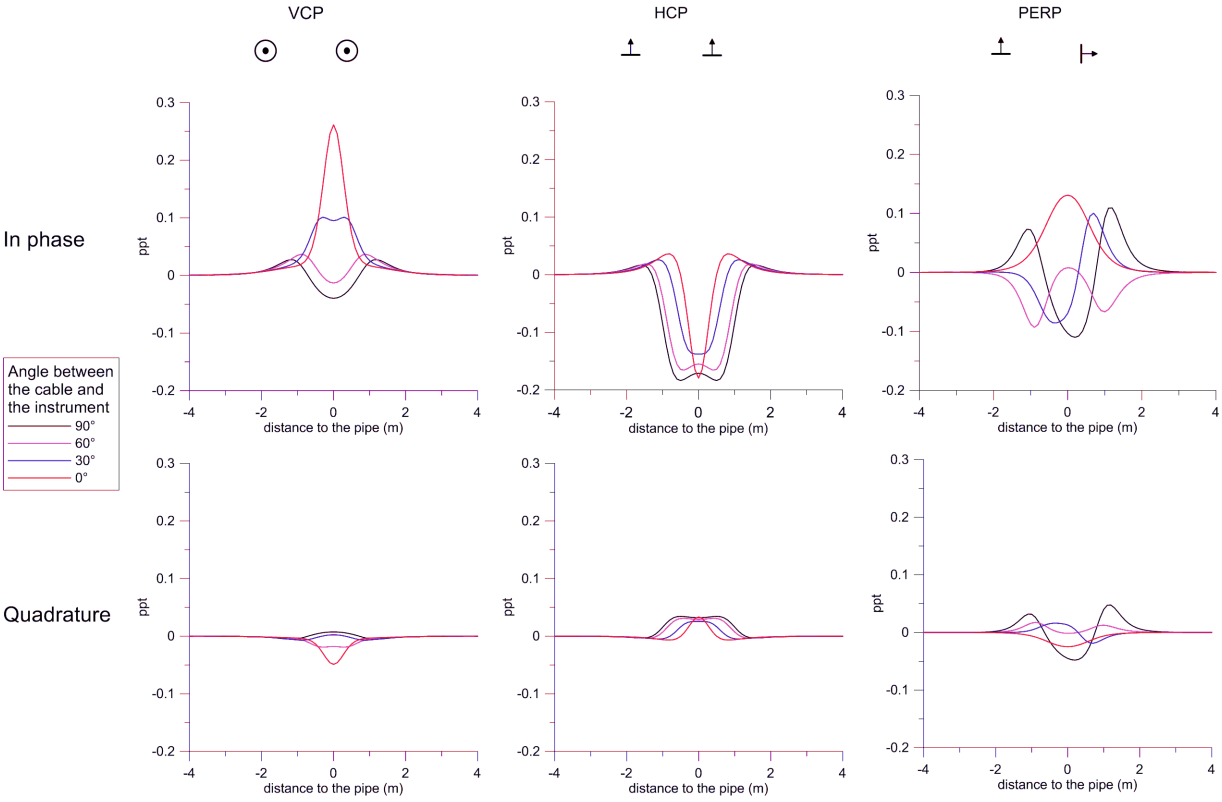

465

466 Fig. 5

467

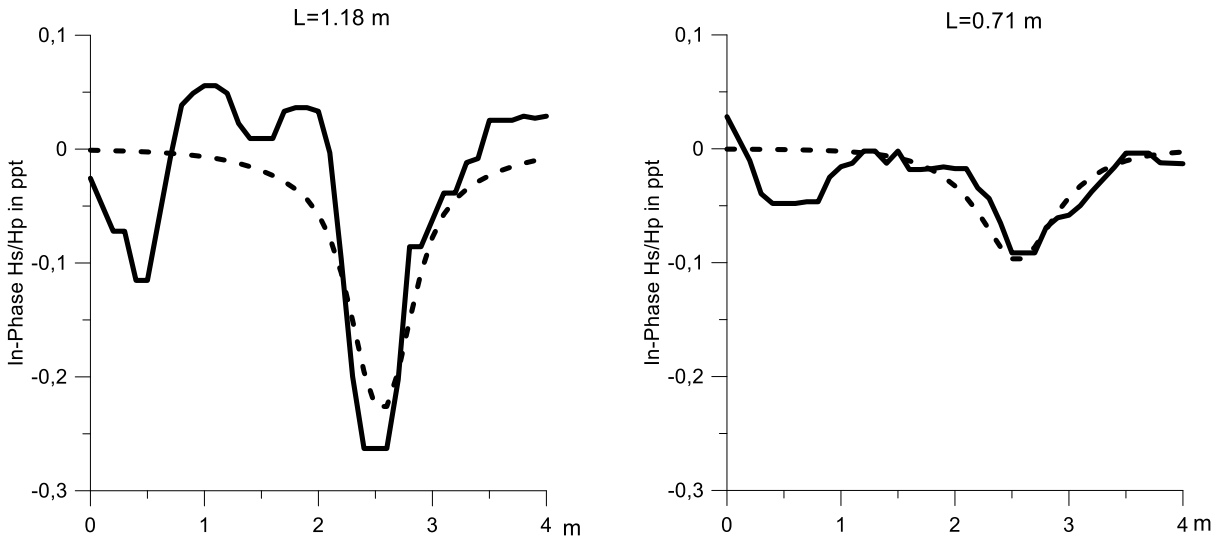

468

469 Fig. 6

470

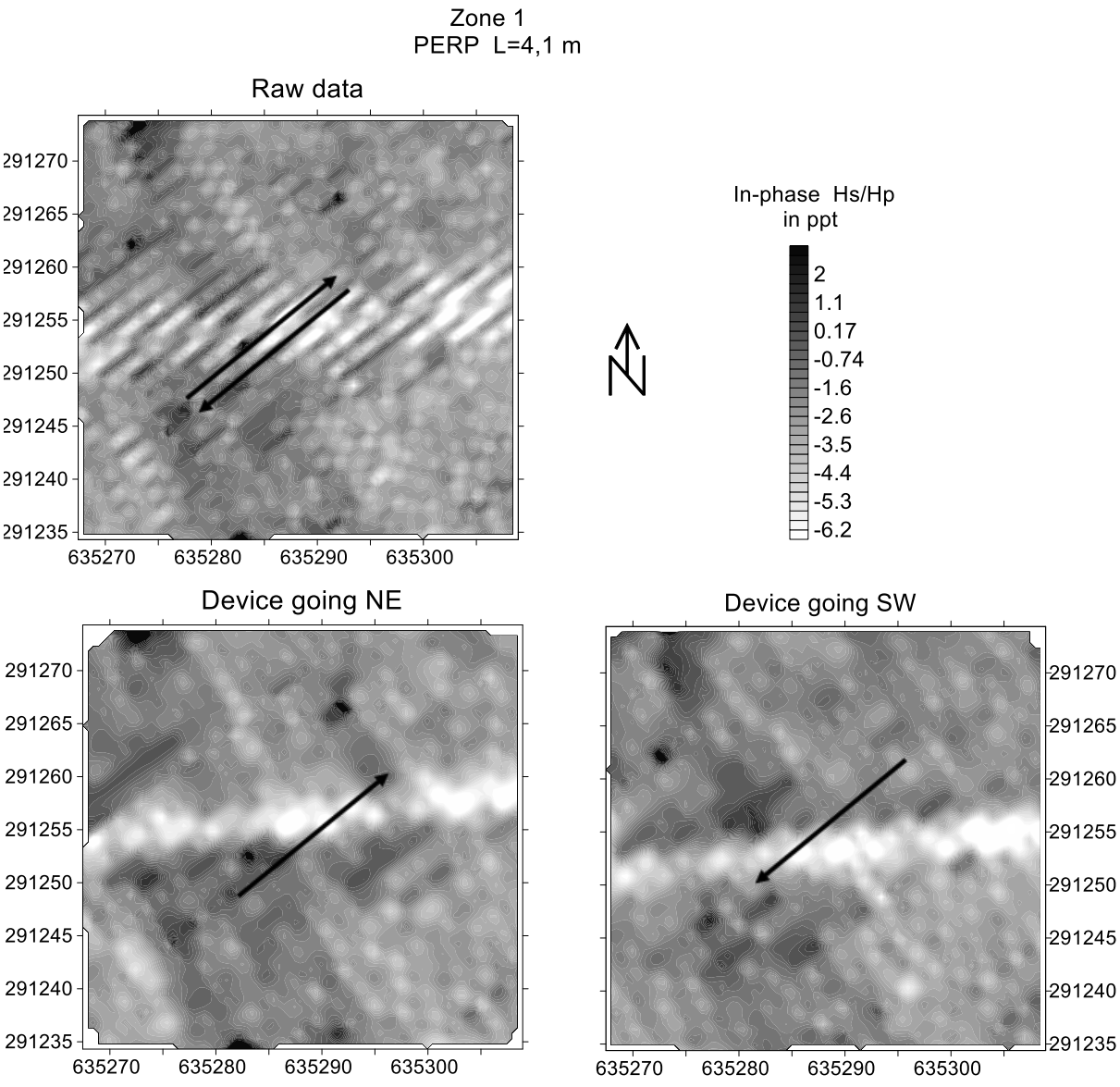

471

472 Fig. 7

473

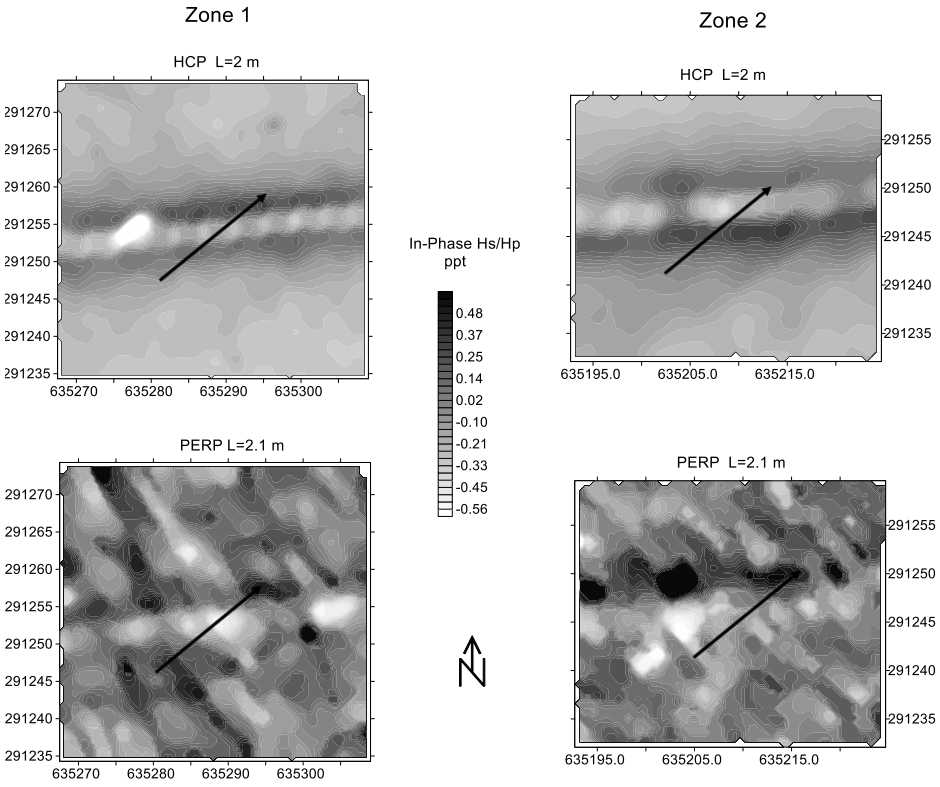

474

475

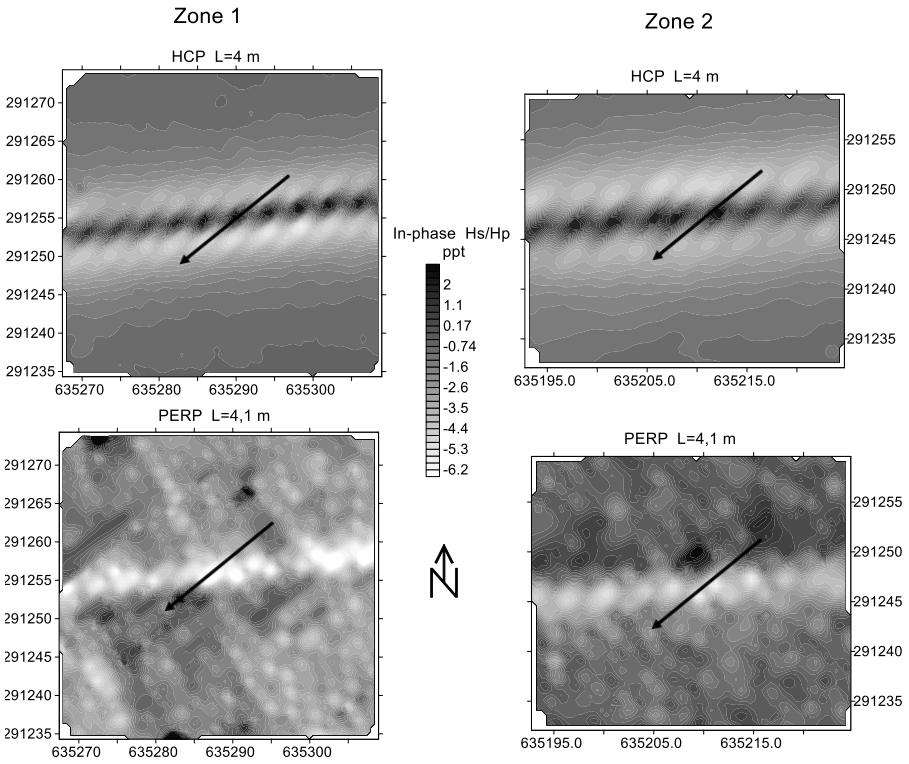

476

477 Fig. 8

478

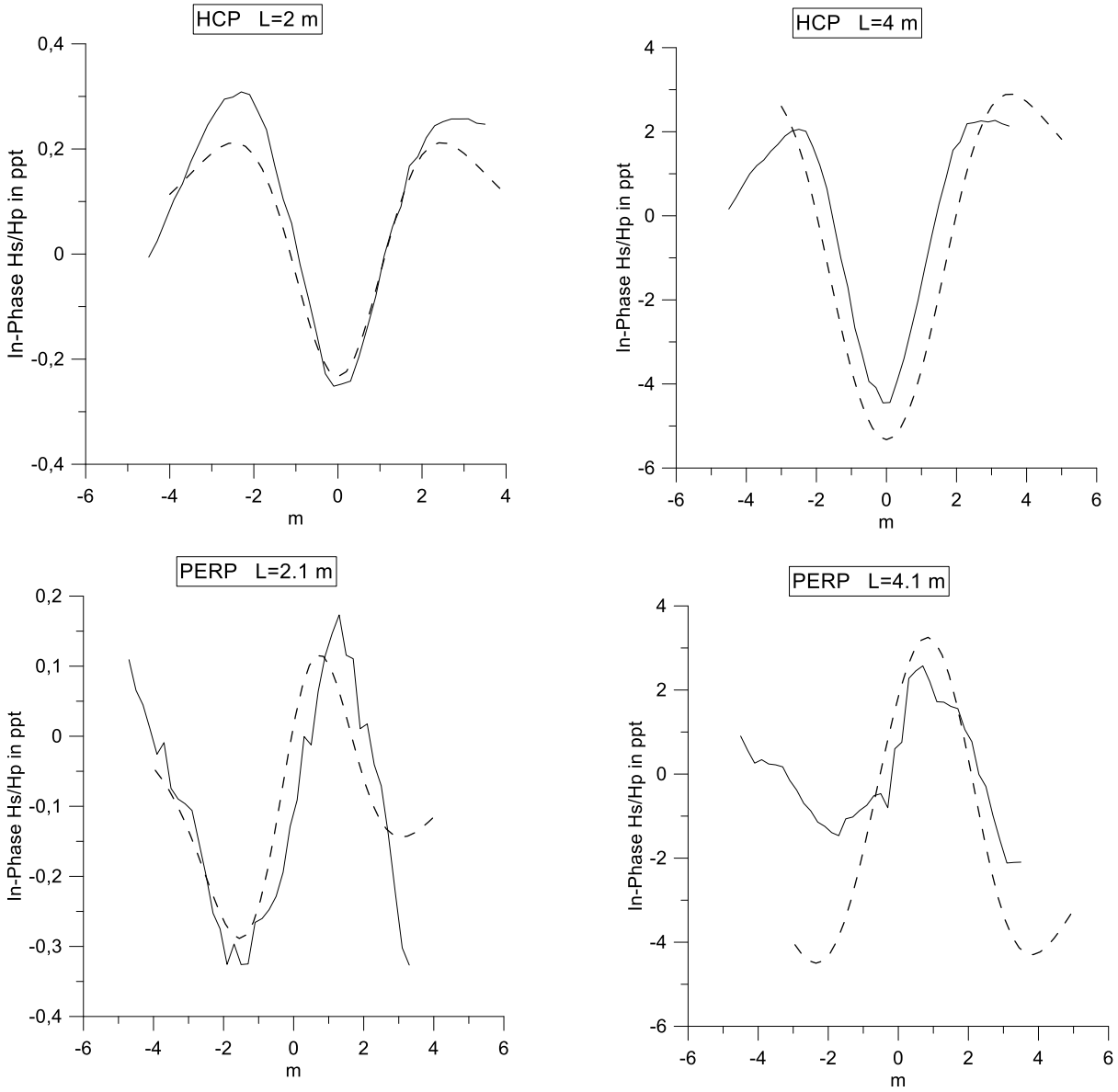

479

480 Fig. 9

481

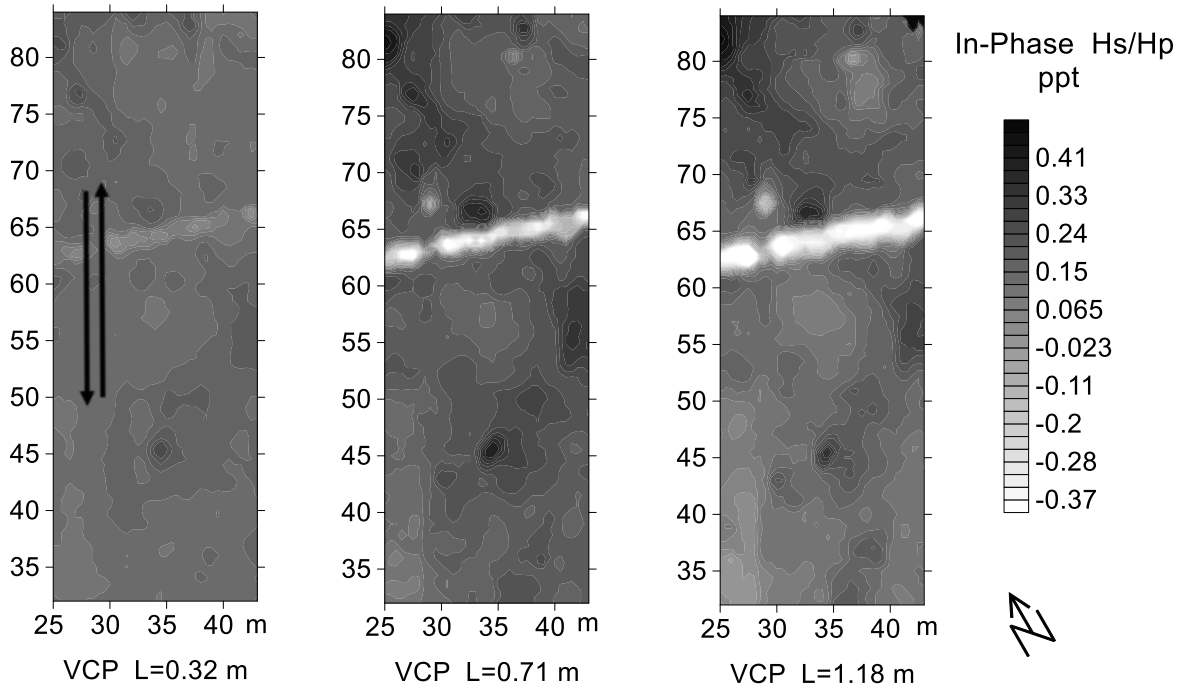

482

483 Fig. 10

484

485

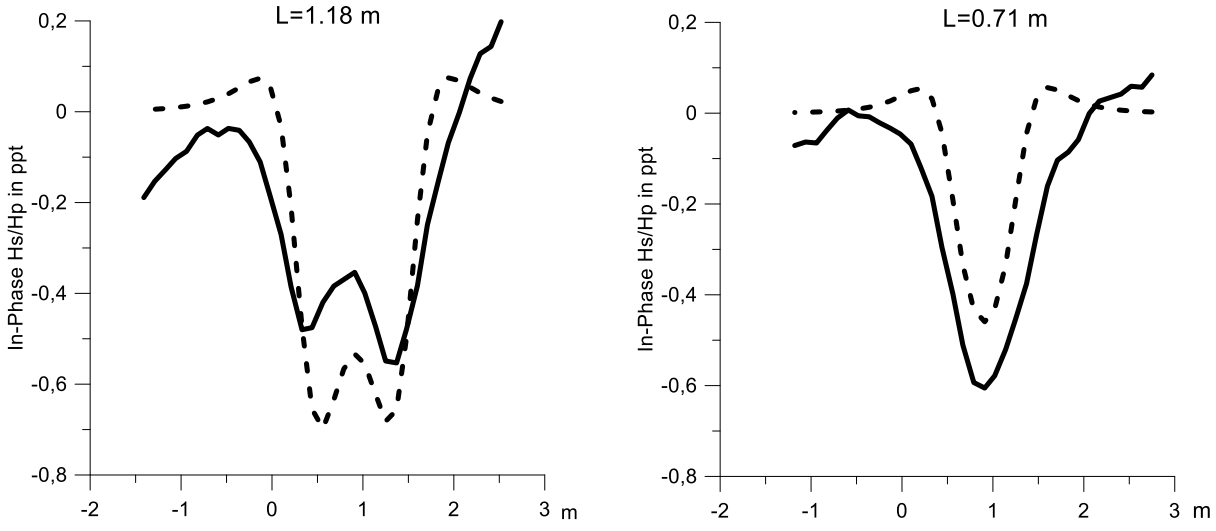

486

487 Fig. 11

488

Device Configuration/ cable depth for 10° cable orientation	Hs/Hp: maximum in-phase cable response in ppt	Hs/Hp: maximum quadrature cable response in ppt	Corresponding apparent magnetic susceptibility variation in 10^{-5} SI	Corresponding apparent conductivity variation in mSm^{-1}
VCP/ 0.5m	-0.182	-0.0794	-38.5	1.41
VCP/ 1m	-0.0385	-0.0168	-8.03	0.30
VCP/ 2m	-0.00357	-0.0016	-0.70	0.026
HCP/ 0.5m	0.133	0.0582	-32.0	-1.0
HCP/ 1m	-0.0112	-0.0049	-0.24	-0.035
HCP/ 2m	-0.00449	-0.00193	1.01	-0.025
PERP/ 0.5m	0.109	0.047	-40.1	0.83
PERP/ 1m	0.0465	0.0202	-17.1	0.35
PERP/ 2m	0.00504	0.00216	-1.85	0.038

Table 1

Device Configuration/ cable depth for 80° cable orientation	Hs/Hp: maximum in-phase cable response in ppt	Hs/Hp: maximum quadrature cable response in ppt	Corresponding apparent magnetic susceptibility variation in 10^{-5} SI	Corresponding apparent conductivity variation in mSm^{-1}
VCP/ 0.5m	0.0292	0.01275	-4.74	0.17
VCP/ 1m	-0.00842	-0.00365	-1.71	0.063
VCP/ 2m	-0.00204	-0.00088	-0.39	0.015
HCP/ 0.5m	0.144	0.0627	-34.5	-1.0
HCP/ 1m	0.0349	0.0152	-8.33	-0.24
HCP/ 2m	-0.00186	-0.0008	0.5	0
PERP/ 0.5m	0.1112	0.0484	-41.0	0.85
PERP/ 1m	0.0318	0.0138	-11.7	0.24
PERP/ 2m	0.00537	0.00233	-1.98	0.040

Table 2